Gas–Solid Fluidization in a Centrifugal Field

Gui-Hua Qian, István Bágyi, Ian W. Burdick, Robert Pfeffer, and Henry Shaw
Dept. of Chemical Engineering, Chemistry and Environmental Science, New Jersey Institute of Technology, Newark, NJ 07102

John G. Stevens
Dept. of Mathematical Sciences, Montclair State University, Montclair, NJ 07043

The nature of fluidization and the behavior of particles in a centrifugal field are discussed. Powders are classified into four groups (A, B, C, and D) following Geldart based on their fluidization behavior. A simple general model, agreeing with conventional fluidized beds and usable for variable ''g,'' is proposed to determine the transition boundary between group A and C particles. The general model for conventional fluidized beds by Foscolo and Gibiloro was used to determine the boundary between group A and B particles, and the semiempirical equation of Molerus for the boundary between group B and D particles in a centrifugal field. Theoretical analysis showed that group A particles can shift to group B, and group C particles can shift to group A under a centrifugal force. Therefore, certain group C particles can be fluidized in rotating fluidized beds. For very high ''g,'' however, such particles shift to group D and cannot be fluidized. Experiments in a horizontal rotating fluidized bed under different ''g'' forces to check the theoretical analysis confirmed that Geldart group C particles (7 μm alumina), which cannot be fluidized in a conventional fluidized bed, can fluidize in a rotating fluidized bed operating at a sufficiently high rotating speed to shift them into group A or B. Similarly, in a series of experiments in a rotating fluidized bed, group A particles behaved as group B.

Introduction

Fluidized beds have many advantages over other solids/fluid processors, such as high heat and mass-transfer rates, temperature homogeneity, and high flowability of particles. Therefore, the behavior of fluidized solid particles has been studied and reported in the literature for over 50 years. Fluidized beds have found many industrial applications; the overwhelming majority of these applications involve gas–solid systems. Fluidized beds are used in industry for physical processes like drying, filtration, or agglomeration (coating and granulation), as well as for catalytic and noncatalytic chemical reactions such as cracking of hydrocarbons, combustion of solid fuels, and roasting of ores. Depending on the process requirements, the particle size of the solid material ranges from under 100 microns for catalytic cracking of hydrocarbons to up to several millimeters for drying of wheat in spouted beds. From experimental observations it has been shown that the fluidizing behavior changes drastically within the broad range of particle sizes and different fluids used in industrial applications.

Early on, Wilhelm and Kwauk (1948) described the stability of a fluidized bed of solids fluidized with either a liquid or a gas. Two modes of fluidization, termed particulate and aggregative fluidization, were observed, depending on the value of the Froude number, $U_{mf}^2/(gd_p)$. Particulate fluidization, which was obtained in solids–water experiments, is characterized by the separation of individual particles much the same as the molecules of a gas. It is a nonbubbling, homogeneous fluidization. By contrast, in aggregative fluidization observed in solids–air experiments, the particles tend to remain aggregated, more closely resembling a liquid than a gas. Gas rises through the bed mainly in the form of bubbles, and the system is heterogeneous. Jackson (1963) developed constitutive equations for both the gas and particle phases that showed that an ideal fluidized bed is always unstable if there are no interaction forces between the particles. Rietema (1973) showed that the cohesive force between particles in contact could stabilize the fluidized bed. According to Geldart (1973),

Correspondence concerning this article should be addressed to R. Pfeffer.

with gas–solid fluidized systems one has to distinguish between four types of powder designated as groups: A, B, C, and D. The distinction between these groups of powder is related to the different fluidization behavior observed for each type of powder.

Many studies have shown that the interaction between particles and between the fluid and the particles are closely linked to the fluidization quality. Mutsers and Rietema (1977b) performed experiments using two different gases (nitrogen and hydrogen) having different densities and viscosities. They also were able to achieve different effective gravity forces (up to 20 "g") by carrying out their experiments in a large centrifuge, but reported experimental results only up to 3.07 "g." They found that the dense-phase porosity and the bubble-point porosity in freely bubbling beds is influenced not only by hydrodynamic effects, but by interparticle forces as well. They also concluded that the effective gravity has an effect on the fluidization stability and is related to fluidization quality.

Generally, fluidization stability and quality is a function of particle size and density, fluid viscosity and density, and drag force, cohesive force, and gravity force. The gravity force is clearly a very important factor, but because almost all fluidization experiments have been conducted in vertical gravity-driven beds (1 "g"), we have not seen any references in the literature analyzing the effect of gravity on particle fluidization stability and quality. This article shows the effect of a variable acceleration field ("gravity") on the Geldart powder classification and analyzes the fluidization quality at different "g" forces. A simple semitheoretical equation, which is in agreement with the literature for conventional gravity-driven fluidized beds, is proposed to determine the boundary transition between group A and group C (group A/C) particles, and it is then applied for different "g." The general model, which was developed for conventional fluidized beds by Foscolo and Gibilaro (1984), is used to determine the boundary transition between group A/B particles. The semiempirical equation of Molerus (1982) is used to determine the boundary transition between group B and group D particles in a centrifugal field.

Powder Classification in a Conventional Gravity-Driven Fluidized Bed

This section reviews the previous work on powder classification in gravity-driven gas–solids fluidized beds. In addition, a new semitheoretical equation is presented for the transition from Geldart group A to group C particles.

Geldart's powder classification

Geldart (1973), in his well-known classification of solids fluidized by gases, empirically found that the behavior of solid particles with respect to their fluidizing properties falls into four groups: A, B, C, and D. These groups are characterized by the mean particle size (d_p) and by the density difference between the particles and the gas ($\rho_p - \rho_f$).

Geldart observed that:

- Powders in group A exhibit dense phase expansion after minimum fluidization and prior to the commencement of bubbling. When the gas supply is suddenly cut off, the bed collapse very slowly. All bubbles rise more rapidly than the interstitial gas velocity.
- Powders in group B bubble at the minimum fluidization velocity. Bed expansion is small and the bed collapses very rapidly when the gas supply is shut off. Most bubbles rise more rapidly than the interstitial gas velocity.
- Powders in group C are difficult to fluidize at all, since the interparticle forces are greater than those that the fluid can exert on the particles.
- Powders in group D can form stable spouted beds. Only the largest bubbles rise more slowly than the interstitial fluidizing gas, so that gas flows into the base of the bubble and out from the top of the bubble.

In most applications of fluidized beds, maximal heat and/or mass transfer between the fluidizing gas and the bed solids is desired. Such transfer is optimal in beds that are uniformly fluidized and not bubbling. For this reason, the fluidization obtained using group A particles is preferable to that using B particles, and both are superior to that realized with group C and group D particles. This ranking forms the basis for our discussion of fluidization quality.

Rietema (1984) pointed out that Geldart's classification is correct only when operating at normal temperatures and pressures and in the earth's gravitational field. Other factors, which must be taken into account, include cohesion, gas viscosity, the adsorption of gas on the particles, and gravitational acceleration. Rietema concludes by saying: "A certain powder which shows A-powder behavior might show B-powder behavior when the effective gravitation is increased or a gas of lower viscosity is used. Similarly, a powder, which shows C-powder behavior, might evince A-powder behavior when a gas of higher viscosity is used."

Criterion for the transition between group A and group C particles

Geldart (1973) defined powders that are in any way cohesive to belong to group C. Normal fluidization of these powders is extremely difficult; the powder lifts as a plug in small-diameter tubes and channels (rat-holes) badly, with the gas passing up through voids extending from the distributor to the bed surface. This difficulty arises because the interparticle forces are greater than the drag force that the fluid exerts on the particle. The interparticle forces are generally the result of very small particle size (van der Waals forces), strong electrostatic charges (Coulombic forces), or the presence in the bed of wet or sticky material (capillary forces). Geldart presented only an empirical curve (with no defining equation) to distinguish between group A and C particles in his classification.

Molerus (1982), derived a semiempirical equation to describe the transition between group A and C particles assuming that the product of the Euler number for fluidization and the Reynolds number is a constant (≈ 5.0) for small Reynolds numbers and the voidage, $\epsilon \approx 0.5$. However, it is uncertain whether this equation can be extended to different accelerations. Therefore, in order to analyze the behavior of the transition between group A and C particles under a centrifugal field, a new semitheoretical equation will be developed.

The critical difference between group A and C particles is that group A particles can be fluidized individually, whereas

group C particles will tend to agglomerate because of interparticle cohesive forces and can be fluidized only as agglomerates. Therefore, we will focus on a single particle inside the bed, which is acted upon by a drag force, a gravity and buoyancy force, and a cohesive force. We will analyze each of these forces separately below.

Drag Force. If the relative velocity between a single particle and the surrounding fluid is u and the drag force on the particle is F_d, then the drag coefficient, C_D, is defined by

$$F_d = C_D \frac{\rho_f u^2}{2} \frac{\pi d_p^2}{4}. \tag{1}$$

At the terminal velocity, u_t, for a single falling particle, the drag force is balanced by the net force due to gravity and buoyancy, giving

$$F_{dt} = C_D \frac{\rho_f u_t^2}{2} \frac{\pi d_p^2}{4} = \frac{\pi d_p^3}{6}(\rho_p - \rho_f) g. \tag{2}$$

Khan and Richardson (1990) have shown that if a particle is in a suspension of like particles supported by a fluid having a superficial flow velocity, u, the drag force on a single particle in the suspension of voidage, ϵ, is $\epsilon^{-4.8}$ times that on a single isolated particle. This applies to both the Stokes' and Newton's law regions. Thus

$$F_{d\epsilon} = C_D \frac{\rho_f u^2}{2} \frac{\pi d_p^2}{4} \epsilon^{-4.8}. \tag{3}$$

Gravitational force W_g and buoyancy force W_b. When the bed is in the fluidized state, it behaves as a fluid and the density of the ''fluidized bed'' (solids and gas) is

$$\rho_a = \epsilon \rho_f + (1 - \epsilon) \rho_p. \tag{4}$$

The buoyancy force W_b on a spherical particle is given by

$$W_b = \frac{\pi d_p^3}{6} \rho_a g = \frac{\pi d_p^3}{6} \left(\epsilon \rho_f + (1 - \epsilon) \rho_p\right) g, \tag{5}$$

and the ''effective weight'' of the particle is

$$W_e = W_g - W_b = \frac{\pi d_p^3}{6} \rho_p g - \frac{\pi d_p^3}{6} \left(\epsilon \rho_f + (1 - \epsilon) \rho_p\right) g = \frac{\pi d_p^3}{6}(\rho_p - \rho_f) g \epsilon, \tag{6}$$

in agreement with Foscolo and Gibilaro (1984).

Cohesive Force. The dominant interparticle force between two particles is the van der Waals force. The van der Waals force between two perfectly spherical and rigid particles of diameter d_1 and d_2 can be expressed as

$$F_c = \frac{A}{12 \delta^2} \frac{d_1 d_2}{d_1 + d_2}, \tag{7}$$

where A is Hamaker's constant, which, for most solids, an average value of $A = 10^{-19}$ J has been calculated (Rietema et al., 1993). Here δ is the distance between the two particles and can be estimated to be between 0.15 and 0.4 nm (Krupp, 1967). Normally δ is taken as 0.4 nm (Iwadate et al., 1998; Zhou and Li, 1999). If we assume that the particles have the same size, $d_1 = d_2 = d_p$, then Eq. 7 becomes

$$F_c = \frac{A}{12 \delta^2} \frac{d_p}{2}. \tag{8}$$

But the calculated cohesive force using Eq. 8 is extremely high (Massimilla and Donsi, 1976; Rietema et al., 1993) when compared to experiment. Most powders, however, have a rather rough surface with many protuberances, generally called asperities, with radii of curvature often not larger than 0.1 μm. Therefore, the value of d_p in Eq. 8 should be replaced by the diameter of the asperities, l (Rietema et al., 1993). This will reduce the value of the cohesion force and make it much more realistic. Thus, the effective average cohesion force depends strongly on the surface structure of the particles, that is, the size distribution of the asperities and their surface density. Massimilla and Donsi (1976) suggest using a mean value of l equal to 0.2 μm, so that Eq. 8 becomes

$$F_c = \frac{A}{12 \delta^2} \frac{l}{2} = \frac{Al}{24 \delta^2}. \tag{9}$$

Transition Equation Between Group A and Group C. Group A particles can be fluidized individually. At the maximum flow velocity, u_m (before the particles flow out of the bed) for group A particles, $F_{d\epsilon} > W_e + F_c$, and for group C particles, since the particles form agglomerates, $F_{d\epsilon} < W_e + F_c$. Figure 1 is a conceptual representation showing all the pertinent forces acting on a particle on the fluidized bed.

The transition equation can be expressed as

$$F_{d\epsilon}|_{u=u_m} = W_e|_{u=u_m} + F_c|_{u=u_m}. \tag{10}$$

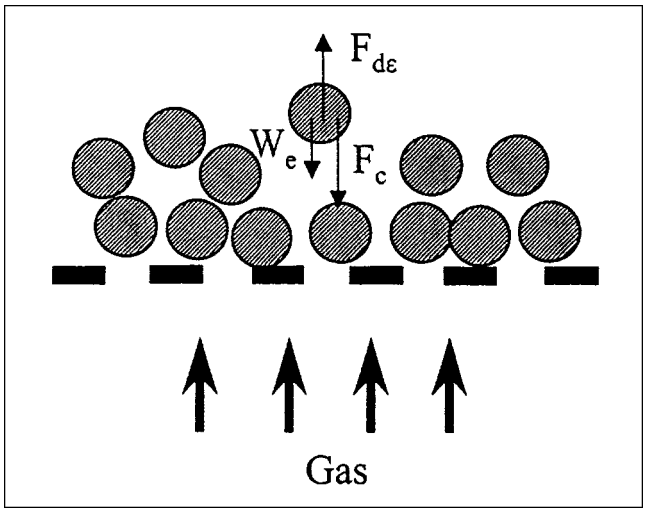

Figure 1. Conceptual representation for transition of group A/C.

If we substitute Eqs. 3, 6, and 9 into Eq. 10, we obtain

$$C_D \frac{\rho_f u_m^2}{2} \frac{\pi d_p^2}{4} \epsilon^{-4.8} = \frac{\pi d_p^3}{6} (\rho_p - \rho_f) g\epsilon + \frac{Al}{24\delta^2}. \quad (11)$$

The maximum velocity before the particles flow out of the bed is $u_m = u_t$. At the terminal velocity u_t,

$$C_D \frac{\rho_f u_t^2}{2} \frac{\pi d_p^2}{4} \epsilon^{-4.8} = \frac{\pi d_p^3}{6} (\rho_p - \rho_f) g\epsilon + \frac{Al}{24\delta^2}. \quad (12)$$

Substituting Eq. 2 into Eq. 12 gives

$$\frac{\pi d_p^3}{6} (\rho_p - \rho_f) g(\epsilon^{-4.8} - \epsilon) = \frac{Al}{24\delta^2}, \quad (13)$$

which is the transition equation for group A/C particles. Here $A = 10^{-19}$ J, $l = 0.2$ μm, $\delta = 0.4$ nm. The voidage for group C particles is different for different materials, and $\epsilon = 0.53$ is used here as an upper limit based on the measurement by Chaouki et al. (1985) for aerogels. The voidage, ϵ, for group A particles is typically 0.4.

For a gas–solid system in a conventional fluidized bed, $g = 9.8$ m/s^2. A plot of Eq. 13 for the voidage range, $\epsilon = 0.53$ and $\epsilon = 0.4$, yields two straight lines on log paper with slope $= -3$, as shown in Figure 2. This figure and all subsequent figures are based on fluidization by air at ambient conditions. The two straight lines bracket the empirical result of Geldart (1973) and are in close agreement with the semiempirical boundary lines for soft and hard particles of Molerus (1982), which represent the transition of group A/C. Thus Eq. 13 is an excellent representation of the transition from group A to group C without requiring the specification of any empirical parameters. It should be noted, however, that Eq. 13 is sensitive to the voidage, and the voidage will change with the particle size. For example, the voidage was found to be as high as 0.67 for 1-μm SiC particles (Zhou et al., 1999). Furthermore, in a centrifugal field, the voidage could be smaller than in a conventional gravity-driven fluidized bed, since the centrifugal force will tend to pack the particles closer together Mutsers et al., 1977a).

We have replaced the particle diameter by the size of the asperities in Eq. 13 to calculate the van der Waals cohesive force, but for very fine particles ($d_p < 0.2$ μm), l should be replaced by d_p.

Criterion for the transition between group A and group B particles

Foscolo and Gibilaro (1984) emphatically rejected the idea that interparticle forces are responsible for the stabilization of a fluidized bed at gas flows below that required to initiate bubbling. Instead, they invoked the stability criterion presented by Wallis (1969) that bubbles occur when conditions

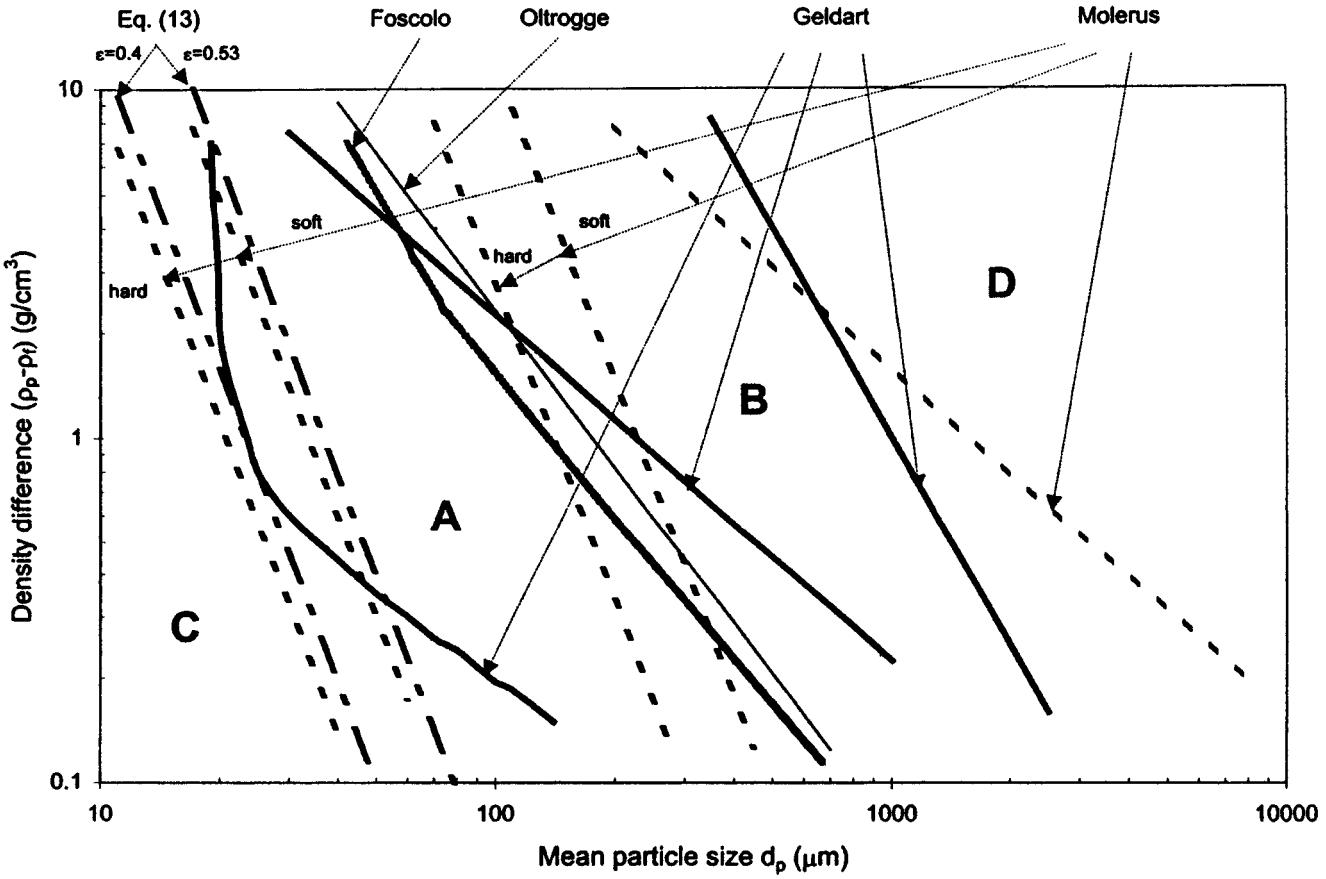

Figure 2. Powder classification for fluidization by air.

are such that the propagation velocity of a voidage disturbance reaches the velocity of elastic waves in the bed. In some respects this idea is analogous to the condition of a projectible reaching the velocity of sound in a fluid. Thus, for voidage propagation velocities smaller than the elastic wave velocity, $u_\epsilon < u_e$, disturbances will be accommodated in an essentially homogeneous manner, whereas for $\mu_\epsilon > u_e$, this is no longer possible and bubbles are formed. This reasoning led to a relatively simple criterion for the instability or transition of Geldart A/B:

$$\frac{(gd_p)^{1/2}}{u_t}\left(\frac{\rho_p-\rho_f}{\rho_p}\right)^{1/2} < 0.56\,n(1-\epsilon_b)^{1/2}\epsilon_b^{n-1}, \quad (14)$$

where ϵ_b is the voidage at which the transition from particulate to aggregative fluidization occurs. For cases of practical interest, $\epsilon_b = \epsilon_{mb}$, where ϵ_{mb} is the voidage at the minimum bubbling velocity. Foscolo and Gibilaro (1984) applied the stability criterion given by Eq. 14 to define the boundary between powders that undergo a degree of particulate expansion ($u_{mb} > u_{mf}$) when fluidized by air and those that do not ($u_{mb} = u_{mf}$).

Equation 14 is dependent on the terminal velocity of a single particle, the Reynolds number, $Re_t = (\rho_f d_p u_t/\mu)$, and n, which comes from the Richardson-Zaki equation (Richardson and Zaki, 1954). The terminal velocity u_t can be obtained from Eq. 2 if the drag coefficient, C_D, is known. The drag coefficient is described as $C_D = 24/Re_t$ for $Re_t < 0.1$ (for engineering purposes, it is often used up to $Re_t < 2.0$), $C_D = 18.5/Re_t^{0.6}$ for $2 < Re_t < 5\times10^2$ and $C_D \approx 0.44$ for $5\times10^2 < Re_t < 2\times10^5$ (Schlichting, 1979). For different Re_t regimes, u_t and n can be expressed mathematically by equations in Table 1 (assuming the particle size is much smaller than the diameter of the fluidized bed, $d_p/D_t \approx 0$).

Inserting the physical properties of air and letting $\epsilon_b = 0.35$, corresponding to the practical minimum value of ϵ_{mf} for spherical particles into Eq. 14, the boundary dividing group A/B powders for conventional gas–solid fluidized beds is obtained and plotted in Figure 2. The curve is in good agreement with the result of Oltrogge (1972), given in Geldart's 1973 article, based on an equation suggested by Verloop and Heerjes (1970), but modified empirically to fit his experimental data. Also shown in Figure 2 are the transition curves between group A/B given by Molerus (1982) for soft and hard particles.

Criterion for the transition between group B and group D particles

Molerus (1982) gave a simple criterion for the transition from group B to group D powders, assuming that the transition occurs with coarse-grained particles at $Re \gg 1$. From the nondimensional representation of the drag exerted on the particles in the high Reynolds number regime, experimental data have shown that the Euler number can be taken to be constant for a given porosity. In particular, at minimum fluidization:

$$Eu_{mf} = \frac{4}{3}\frac{d_p(\rho_p-\rho_f)g\epsilon_{mf}^2}{\rho_f u_{mf}^2} = \text{constant}. \quad (15)$$

With $\epsilon_{mf} \approx 0.5$, $\epsilon_{mf}^2 = 0.25$, $Eu_{mf} \approx 5$,

$$\frac{d_p(\rho_p-\rho_f)g}{\rho_f u_{mf}^2} \approx 15. \quad (16)$$

According to Molerus, this result has a simple physical meaning. With high Reynolds number and therefore dominance of the inertia forces in comparison with viscous forces, the dynamic pressure of the fluid, $\rho_f u_{mf}^2$, must exceed a certain value with onset of fluidization in comparison with the particles' weight minus buoyancy. From that consideration, it is reasonable to assume that such systems tend to spout for which the dynamic pressure of the fluid exceeds a critical value $\rho_f u_{mf}^2 = \text{constant}$, so that with onset of fluidization Eq. 16 can be written as

$$d_p(\rho_p-\rho_f)g = \text{constant}. \quad (17)$$

Table 1. Equations to Calculate n and u_t for Different Re_t

Re_t	n	u_t
$Re_t < 0.2$	$n = 4.65 + 20\left(\frac{d_p}{D_t}\right) \approx 4.65$	$u_t = \frac{d_p^2(\rho_p-\rho_f)g}{18\mu}$
$0.2 < Re_t < 1.0$	$n = \left[4.35 + 1.75\left(\frac{d_p}{D_t}\right)\right]Re_t^{-0.03} \approx 4.35\,Re_t^{-0.03}$	$u_t = \frac{d_p^2(\rho_p-\rho_f)g}{18\mu}$
$1.0 < Re_t < 2.0$	$n = \left[4.45 + 18\left(\frac{d_p}{D_t}\right)\right]Re_t^{-0.1} \approx 4.45\,Re_t^{-0.1}$	$u_t = \frac{d_p^2(\rho_p-\rho_f)g}{18\mu}$
$2.0 < Re_t < 200$	$n = \left[4.45 + 18\left(\frac{d_p}{D_t}\right)\right]Re_t^{-0.1} \approx 4.45\,Re_t^{-0.1}$	$u_t = 0.153\frac{d_p^{1.14}[(\rho_p-\rho_f)g]^{0.71}}{\mu^{0.43}\rho_f^{0.29}}$
$200 < Re_t < 500$	$n = 4.4\,Re_t^{-0.1}$	$u_t = 0.153\frac{d_p^{1.14}[(\rho_p-\rho_f)g]^{0.71}}{\mu^{0.43}\rho_f^{0.29}}$
$Re_t > 500$	$n = 2.39$	$u_t = 1.74\left[\frac{d_p(\rho_p-\rho_f)g}{\rho_f}\right]^{0.5}$

Using the experimental data by Mathur (1971), the final result for the transition of group B to group D particles from Eq. 17 is obtained as

$$d_p(\rho_p - \rho_f)g = 15.3 \text{ N/m}^2. \quad (18)$$

This result is plotted in Figure 2 and agrees well with the experimental data reported by Geldart (1973). However, it should be noted that for smaller Reynolds numbers, for example, $Re \approx 1$, Eu_{mf} is no longer constant, and therefore Eq. 18 may not apply.

Powder Classification in a Centrifugal Field

Here we will extend the results presented in the previous section for the classification of powders in gravity-driven fluidized beds to apply to fluidized beds in a centrifugal field, that is, in rotating fluidized beds (RFB).

Criterion for the transition between group A and group C particles

Equation 13 is our semitheoretical result for the transition from group A to group C particles. The g in the equation refers to the gravitational acceleration acting on the particles. In a centrifugal field, g will be replaced by the centrifugal acceleration, a, which will be given in nondimensional form as "g"$= a/(9.8 \text{ m/s}^2)$.

Figure 3 shows the calculated boundary for the transition of group A and C particles at 1 "g," 10 "g," 100 "g," and 1,000 "g." It shows that the boundary curve shifts to the left with increasing "g." It can be seen, for example, that particles exist (of specific size and density) that belong to group C at 1 "g," but belong to group A at 10 "g." The figure also shows that it should be possible to fluidize some group C particles without agglomeration in a centrifugal field, depending on the value of "g."

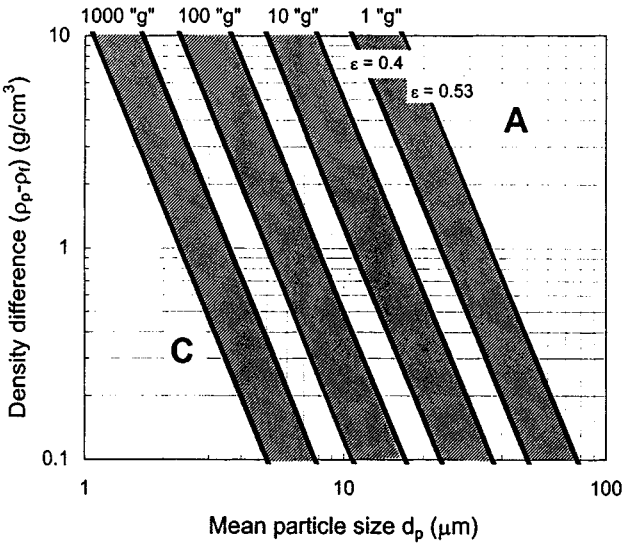

Figure 3. Group A/C transition for fluidization by air at different " *g*."

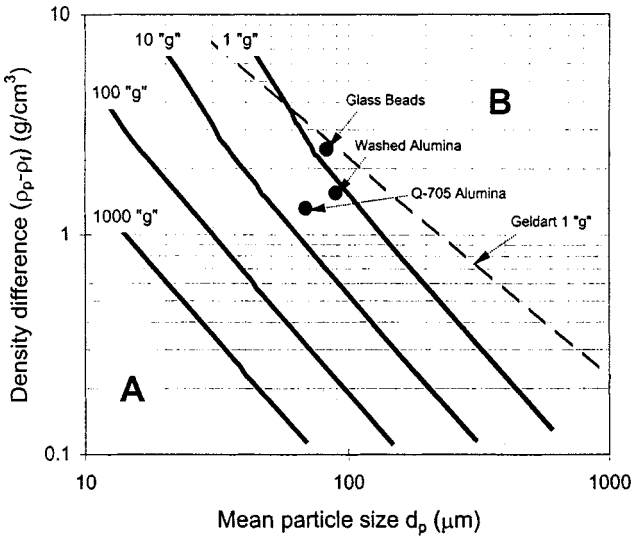

Figure 4. Group A/B transition for fluidization by air at different " *g*."

Criterion for transition between group A and B particles

Equation 15, suggested by Foscolo and Gibilaro (1984), is also seen to be dependent on the gravitational acceleration. In a centrifugal field, the gravitational acceleration is replaced by the centrifugal acceleration and Eq. 14 can be modified accordingly. Figure 4 shows the calculated boundary transition curves for group A and B particles at 1 "g," 10 "g," 100 "g," and 1,000 "g." It shows that the boundary curve shifts to the left with increasing "g." Thus, if group A particles can shift to group B in a centrifugal field and the additional centrifugal force (above 1 "g") will reduce the fluidization quality for group A particles.

Criterion for transition between group B and D particles

Equation 18 suggested by Molerus (1982) is used to calculate the transition from group B/D in a centrifugal field. Figure 5 shows the calculated boundary transition curves for group B/D at different "g." Therefore, group B particles can shift to group D, which are not easy to fluidize and tend to spout in a conventional fluidized bed. Figure 5 also shows that group D particles can shift to group B or even to group A if "g" is less than unity. Thus, by decreasing "g," group B particles can shift to group A, and group D particles can shift to group B or to group A. Group D particles are large or dense and are difficult to fluidize. However, if they shift to group B or A, the fluidization quality of group D particles will be improved. This effect can be achieved by fluidization under microgravity conditions such as fluidizing particles on the moon, or by applying an external force, such as a magnetic or electric field to balance the gravity force.

Experiments

In order to test the ideas and equations developed for the classification of powders in a centrifugal field presented earlier, a series of experiments was performed in a rotating fluidized bed where the centrifugal acceleration could be varied from 7 "g" to over 200 "g."

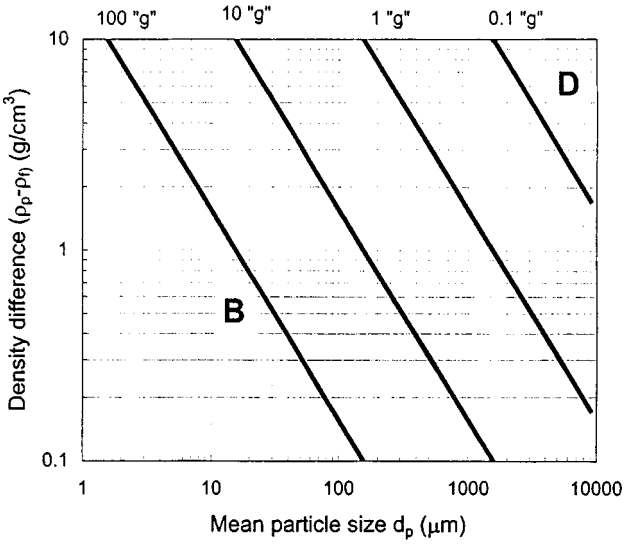

Figure 5. Group B/D transition for fluidization by air at different " *g*."

Rotating fluidized bed

Unlike in a conventional gravity-driven fluidized bed, where the distributor is situated horizontally, in an RFB the distributor is a cylinder, either horizontal or vertical, that rotates around its axis of symmetry. Figure 6 is a schematic diagram of a horizontal RFB. Particles inside the distributor are forced to the wall due to the large centrifugal forces produced by the rotation. Instead of having a fixed gravitational field as in a conventional fluidized bed, the centrifugal force, that is, acceleration, becomes an adjustable parameter that is determined by the rotational speed and the bed radius. Thus in a rotating fluidized bed, the minimum fluidization velocity increases as the rotating speed is increased so that bubble formation can be avoided even at very high flow rates, resulting in improved gas–solid contact.

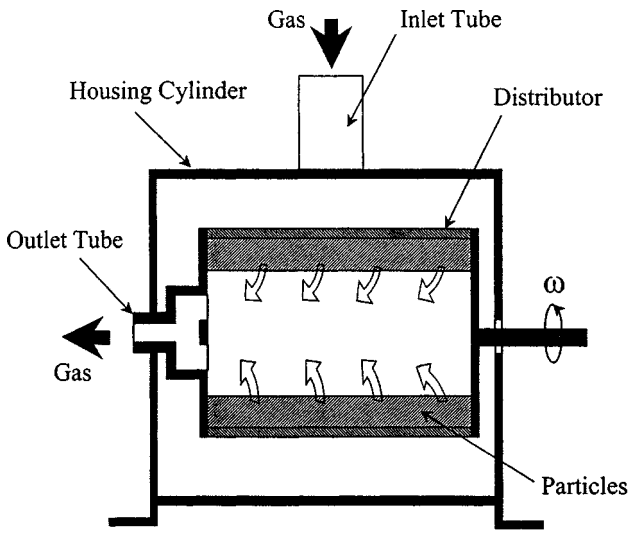

Figure 6. Rotating fluidized bed.

Rotating fluidized beds have been studied both theoretically and experimentally for many years (see, for example, Levy et al., 1978, 1981; Kroger et al., 1980; Fan et al., 1985; Kao et al., 1987; Chen, 1987; Qian et al., 1998, 1999). The theoretical analysis by Chen (1987) is based on local momentum balances. Unlike previous theories, the voidage of the particle bed is allowed to vary so that the transition from a packed to a fluidized bed can be easily followed and the fluidizing condition is clearly defined. In his analysis, Chen assumed that the slip velocity between the two phases is equivalent to the gas velocity and that the particles rotate as a solid body. Chen was also the first to point out that rotating fluidized beds, unlike conventional fluidized beds, fluidize layer by layer, from the inner surface outward as the gas velocity is increased. The theory also predicts that the pressure drop should reach a plateau beyond the critical fluidization velocity when the entire bed is fluidized.

We have previously investigated the nature of fluidization and discussed novel applications of rotating fluidized beds, for example, as dust filters or as catalytic reactors for the cleanup of diesel exhaust (Qian et al., 1998, 1999). Depending on the application and the aerosol to be treated, the size and composition of bed particles may vary widely. For example, for the treatment of diesel exhaust we have used larger (~ 80 μm) granules of zeolite catalyst mixed with silica/alumina and are now investigating the use of much smaller (~ 5 μm) catalyst particles.

Experimental system

The experimental system used in our research is shown in Figure 7. Dry compressed air was fed to the RFB through a bank of calibrated rotameters. A variable-speed motor provided rotating speeds between 0 and 5,000 rpm. The metal distributor (manufactured by Pall Corporation) was composed of sintered 316 low-carbon stainless-steel powder with an average pore size of 55 μm. Its length was 15.2 cm, with an inner radius (the same as the outer radius of the bed) of 6.15 cm. Plexiglas end plates were used so that the bed and bed surface could be observed by eye or by a high-resolution digital camera.

The rotating speed of the RFB was set at 325, 525, 700, 900, 1,200 1,600 and 2,000 rpm (34, 55, 73, 94, 126, 167 and 209 rad/s), which is equivalent to a centrifugal acceleration of 7, 19, 34, 56, 100, 178 and 278 "*g*," respectively. The strobe

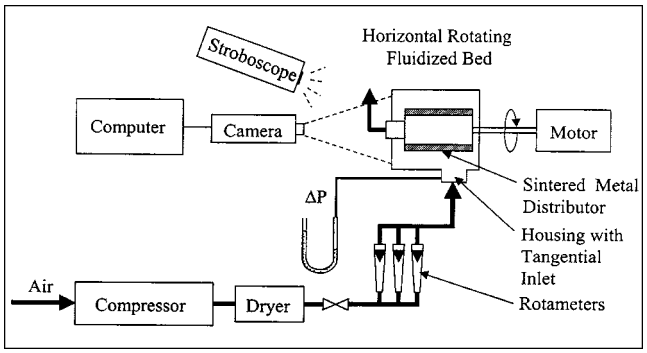

Figure 7. Experimental system.

frequency was set to match the rotational frequency of the bed so that any macroscopic bubbles present could be observed. The pressure drop as a function of gas velocity and rotating speed was measured using a U-tube water manometer. Before loading particles into the bed, the pressure drop of the distributor of the empty bed was also measured and then subtracted from the measured pressure drop of the bed loaded with particles.

Our experiments were conducted with Geldart A and C particles, with properties liested in Table 2. The bed material consisted of glass beads provided by MO-SCI Corporation and alumina provided by the Alcoa Technical Center. The particle-size distribution for all of these particles was measured using an Aerosizer (Amherst Process Instruments, Inc.); typical reuslts are shown in Figure 8. The fresh alumina has a broad size distribution with many fines; washed alumina has far fewer fines. The glass beads have a much narrower size distribution than the alumina particles and a higher density. The 7-micron alumina particles, due to their small size, belong to Geldart group C; all the others belong to Geldart group A.

Table 2. Particle Properties

Particle	Particle Dens. (kg/m^3)	Mean Part. Dia. by Vol. (μm)	Mean Part. Dia. by No. (μm)	Geldart Group
Glass beads	2,450	82	75	A
Washed alumina	1,550	89	28	A
Fresh alumina	1,550	63	4	A
Q-705 alumina	1,320	68	48	A
7-μm alumina	1,470	7	2	C

Experimental results

Experiments were conducted by measuring the pressure drop of the bed as a function of gas velocity and rotating speed. Visual observations of the minimum fluidization and minimum bubbling velocity, and the quality of fluidization were made by eye and by high-resolution photography.

Group A Particles. The most easily observed difference between powders in groups A and B is whether or not the bed bubbles at or very close to minimum fluidization. The minimum bubbling velocity is defined as the gas velocity when bubbles are first observed. At low gas flow rate the bed is in the packed-bed regime. As the gas velocity is increased, the inner surface begins to fluidize (Qian et al., 1998). The inner surface fluidizes first because at that point the gas velocity in the bed is highest and the centrifugal force is lowest. The velocity at which fluidization occurs at the inner surface is called the inner surface fluidization velocity, (U_{mfi}). After U_{mfi} is reached, bubbles are first observed. Figure 9 shows the pressure drop for a 0.5-kg charge of washed alumina particles as a function of the gas flow rate at different rotating speeds. At rotating speeds greater than 325 rpm, the minimum bubbling velocity, U_{mb}, was observed before the critical minimum fluidization velocity (U_{mfc}) was reached, that is, when the entire bed has fluidized. At the rotating speed of 325 rpm, the values of U_{mb}, U_{mfi}, and U_{mfc} are practically the same.

Similar experiments have been conducted using Q-705 alumina particles and glass beads. Figures 10 and 11 show the

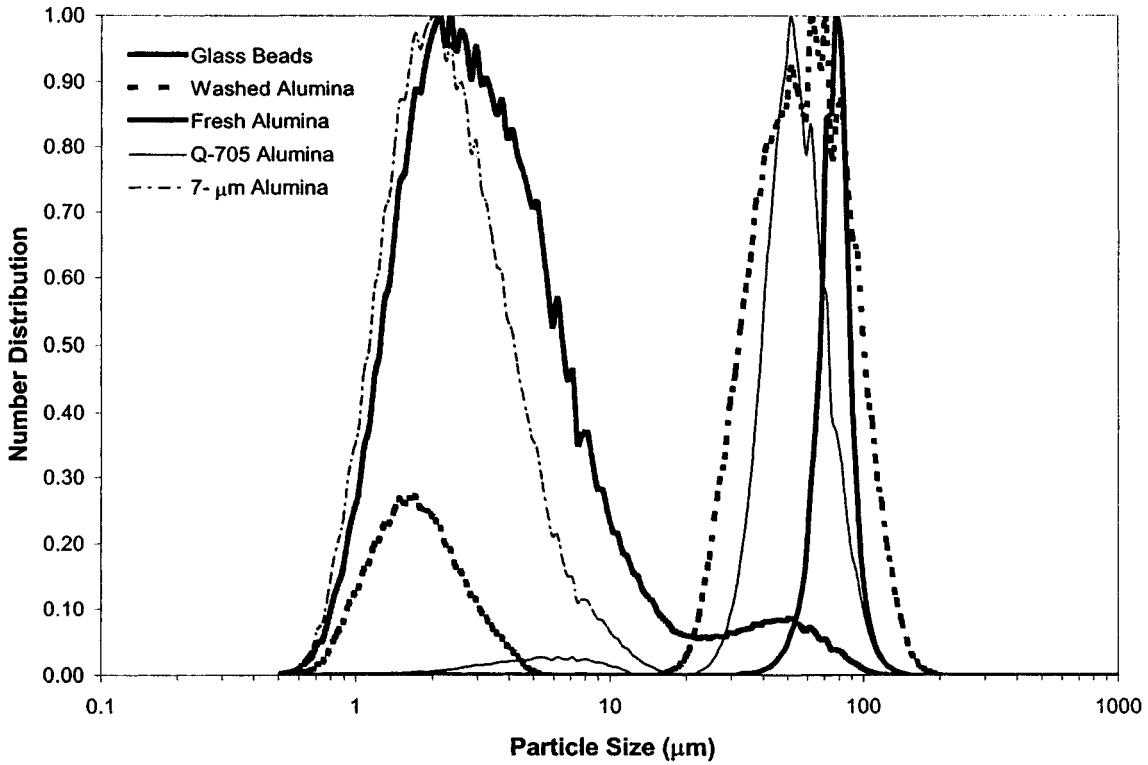

Figure 8. Particle-size distribution.

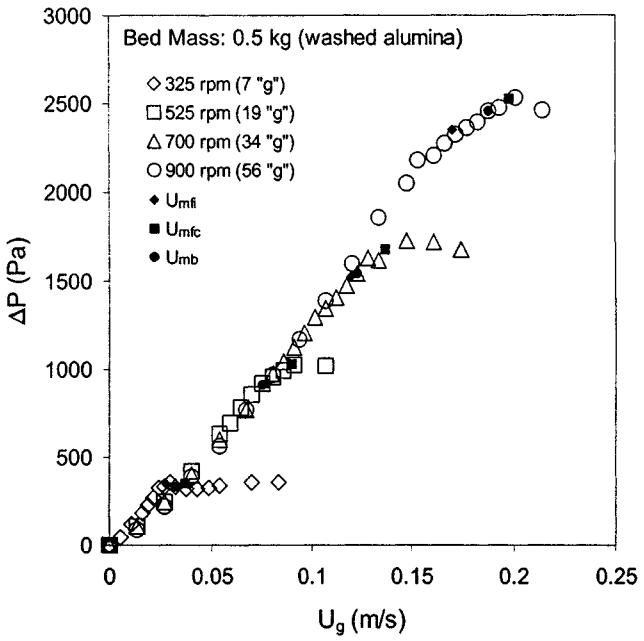

Figure 9. Pressure drop due to a 0.5-kg charge of washed alumina particles as a function of flow rate at 325, 525, 700 and 900 rpm.

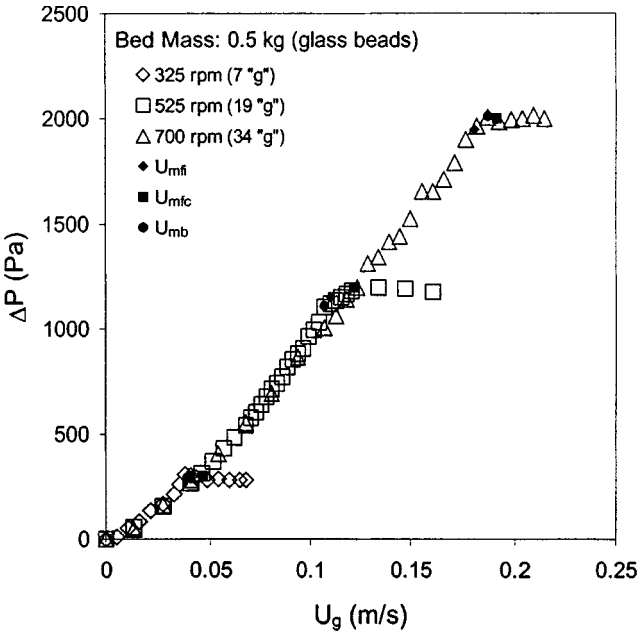

Figure 11. Pressure drop due to a 0.5-kg charge of glass beads as a function of flow rate at 325, 525, and 700 rpm.

pressure drop for a 0.5-kg charge of Q-705 alumina particles and 0.5-kg charge of glass beads, respectively, as a function of flow rate at different rotating speeds. As seen in the figures, the results are very close to those obtained using the washed alumina.

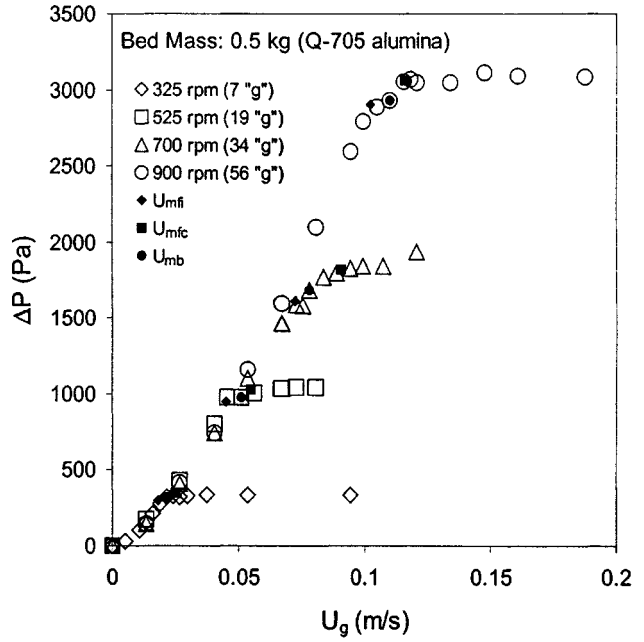

Figure 10. Pressure drop due to a 0.5-kg charge of Q-705 alumina particles as a function of flow rate at 325, 525, 700 and 900 rpm.

The preceding experiments indicate that in all cases U_{mf} and U_{mb} are very close or practicaly equal. Here U_{mf} is the average of U_{mfi} and U_{mfc}. In Figure 4, we have marked the mean size and density of the particles used in each of the previous experiments. According to the figure, for all of our centrifugal accelerations ("g"), the particles behave as Geldart group B. However, in Geldart's classification, for a gravity-driven bed, these particles should behave as group A. Thus our experiments imply that group A particles can shift to group B in a centrifugal field.

Effect of Fines. Geldart and Abrahamsen (1980) studied the effect of fines on the behavior of conventional gas-fluidized beds. They found that the presence of a small mass fraction of fines below 45 μm strongly affects and increases the ratio U_{mb}/U_{mf}. Using fresh alumina particles, which contain significant fines below 45 μm, we measured the pressure drop of the bed and observed the onset of bubbling, U_{mb}. Figure 12 shows the pressure drop for a 0.5-kg charge of fresh alumina particles as a function of flow rate at different rotating speeds. It is clear, especially at the higher rotating speeds, that U_{mb} is higher than U_{mfc}. Thus the presence of fines causes the powder to exhibit group A behavior even in the presence of the centrifugal field.

Fluidization of Group C Particles. The ability to fluidize group C particles is potentially significant because of the rapidly growing need for using ultrafine particles in industrial applications. There are two basic methods to improve the fluidization quality of fine cohesive group G particles. One is by application of an external force, such as vibration or from a magnetic, electric, or acoustic field. The other is by altering the intrinsic properties of the particles, for example, modifying their surface characteristics or mixing them with other particles having different size or shape (Wang et al., 1998;

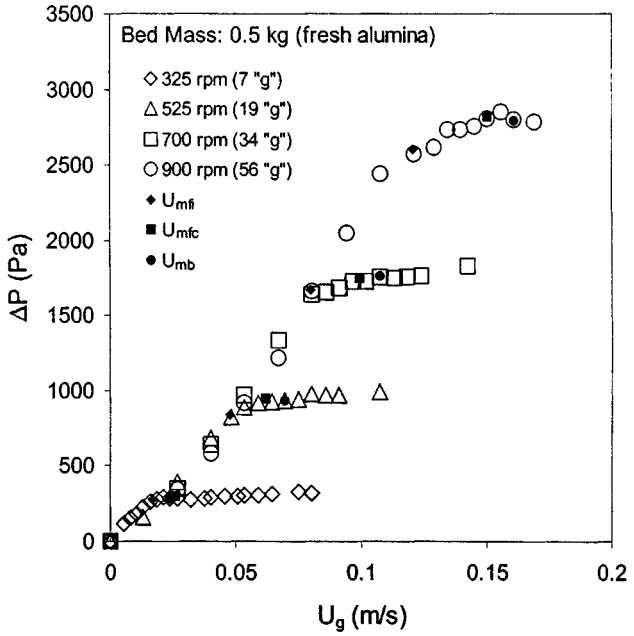

Figure 12. Pressure drop due to a 0.5-kg fresh alumina particles charge as a function of flow rate at 325, 525, 700 and 900 rpm.

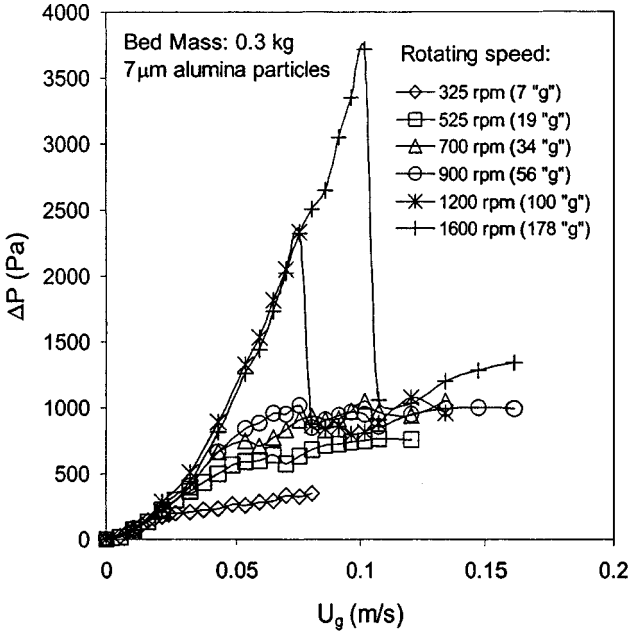

Figure 13. Pressure drop due to a 0.3-kg charge of 7 μm alumina particles as a function of flow rate at 325, 525, 700, 900, 1,200 and 1,600 rpm.

Mori et al., 1992; Chirone et al., 1992; Zhu et al., 1994; Tung et al., 1989). From the theoretical analysis presented earlier, we have shown that group C particles can shift to group A in a centrifugal field and thus can be more easily fluidized. This is a new approach to improving the fluidization quality of fine particles and requires experimental verification.

We therefore carried out experiments in our rotating fluidized bed using 7-μm Geldart group C alumina particles. These particles normally tend to agglomerate. In our experiments, a 0.3-kg charge of the 7-μm alumina particles was loaded into the RFB. The rotating speeds were set at 325, 525, 700, 900, 1,200, 1,600 and 2,000 rpm, equivalent to 7, 19, 34, 56, 100, 178 and 278 "*g*," respectively. At each rotating speed, the pressure drop of the bed was measured as a function of gas flow rate. The strobe frequency was set to match the rotational frequency of the bed, and the bed condition was observed by eye.

Figure 13 shows the measured pressure drop in the bed as a function of flow rate at different rotating speeds. Figure 14 summarizes our observations of the bed condition corresponding to the last data point at each rotating speed shown in Figure 13.

At 325 rpm (7 "*g*") and 525 rpm (19 "*g*"), the particles are observed to be agglomerated and the bed surface is nonuniform. At higher gas velocity, the gas passes through large regular channels, which are somewhat smaller at higher rpm. This is a normal observation for group C particles in a conventional fluidized bed. The pressure drop increases with gas velocity in the packed-bed regime until the pressure drop curve reaches a plateau due to channeling.

At 700 rpm (34 "*g*"), the particles appear to have deagglomerated in the bed, although the bed surface is still not completely uniform. At higher gas velocity, very small chan-

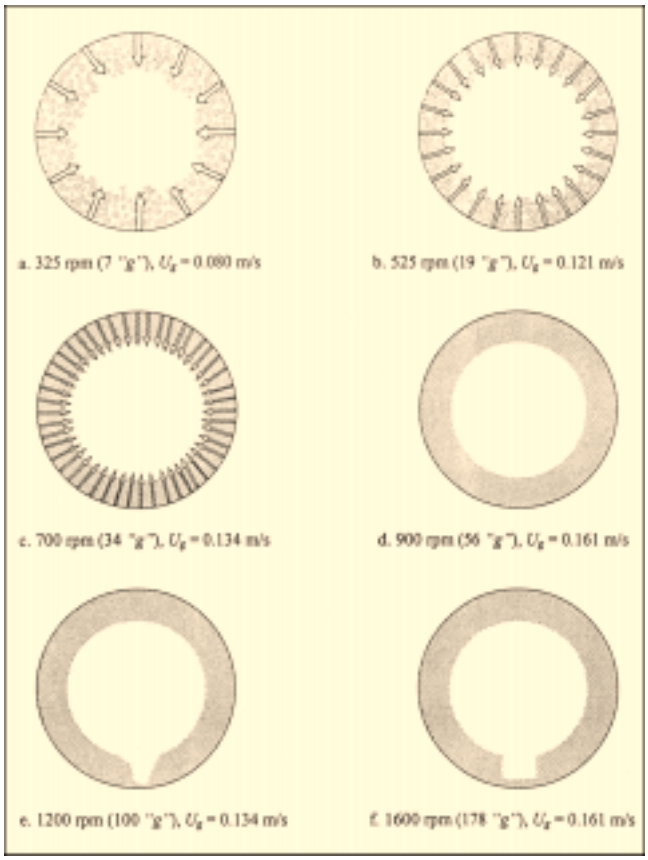

Figure 14. Visual observation of the powder in the RFB corresponding to the data point at the highest velocity shown in Figure 13.

nels could still be observed. It is hard to say whether the particle behavior belongs to group C or group A.

At 900 rpm (56 "*g*") the particles have totally deagglomerated and the bed surface is uniform. At higher gas velocity, the particles behave like group A or B particles and the bed appears uniformly fluidized without channeling, as illustrated in Figure 14d. Distinguishing between group A and group B behavior in these experiments is difficult. The essential difference is whether there exists an interval of gas velocity in which the bed is fully fluidized, but not bubbling. This determination requires careful visual observation and can involve some ambiguity. It is especially difficult if the difference between U_{mf} and U_{mb} is small. For this reason we have labeled as AB the region in which either group A or group B behavior would be expected.

In Figure 13 the pressure drop increases with gas velocity in the packed-bed regime and goes to a plateau after minimum fluidization is reached. Thus, between 700 and 900 rpm, the particles shift from group C to group A or B (region AB) behavior.

At 1,200 rpm (100 "*g*") and 1,600 rpm (178 "*g*"), the bed surface is very uniform in the packed-bed regime because of the high rotating speed. The pressure drop increases steadily, then, as the gas flow is further increased, it decreases suddenly. At this point, a "rat-hole" is observed inside the bed. The gas passes through the rat-hole instead of flowing between the particles. The difference between operating at 1,200 rpm and 1,600 rpm is that the rat-hole size at 1,600 rpm is larger than that at 1,200 rpm. The gas velocity, at which the pressure drop suddenly falls due to the formation of the rat-hole at 1,600 rpm, is higher than that at 1,200 rpm. Similarly, the rat-hole size at 2,000 rpm (278 "*g*") is even larger than at 1,600 rpm and the corresponding gas velocity, when the pressure drop suddenly falls, is higher. These results indicate that the particles are not easy to fluidize at high centrifugal force. It should be noted at that at very high rpm the pressure drop curve looks like that obtained for group D particles rather than for group A and B particles.

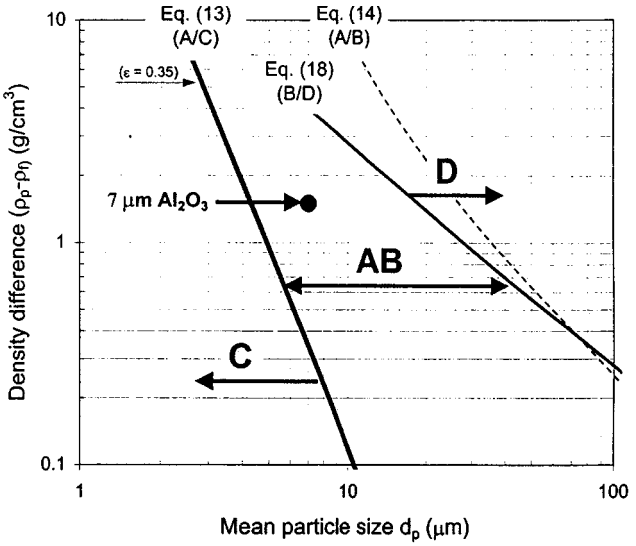

Figure 15. Powder classification for fluidization by air at 56 " *g*."

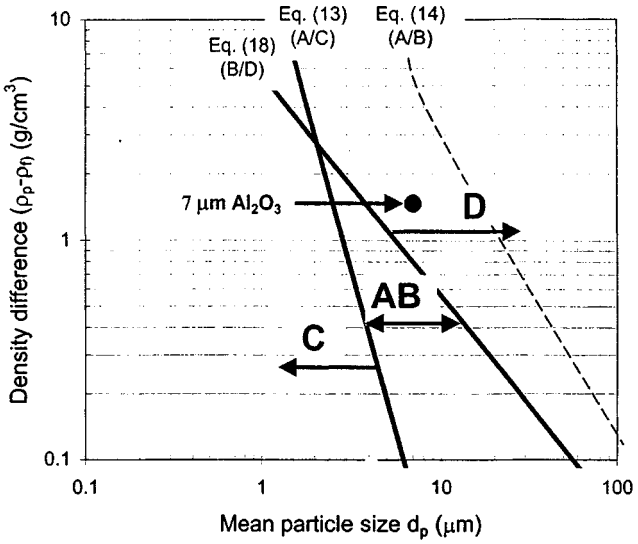

Figure 16. Powder classification for fluidization by air at 278 " *g*."

Since the voidage in the bed is probably lower than 0.4 due to the centrifugal field (Mutsers et al., 1977b), we used a voidage of 0.35 for the transition curve between group A and C. Figure 15 shows that we can see that the transition boundary between group B/D has shifted further to the left than the transition boundary between group A/B. Thus there is no transition between group A and B at high "*g*." Therefore, the 7-μm alumina group C particles shift directly into region AB. In Figure 16, which shows the results at a rotating speed of 2,000 rpm (278 "*g*"), the 7-μm alumina particles have shifted from group C to group D. This observation is consistent with our inability to obtain good fluidization of the 7-μm alumina particles at rotating speeds of 1,200 (100 "*g*"), 1,600 (178 "*g*") and 2,000 rpm (278 "*g*"). We note, however, that although the transition curve (region AB to D) was derived by Molerus (1982) for $Re \gg 1$, our experimental data were obtained at $Re \approx 1$.

Discussion

It is clear from both our theoretical analyses and our experimental results in the RFB that Geldart's powder classification cannot be used in centrifugal fields without modification to take into account gravity forces greater than 1 "*g*." As discussed in Iwadate and Horio (1998), cohesive group C particles can only be fluidized in the form of agglomerates. They define this type of fluidization as "agglomerating fluidization." Agglomerating fluidization is not easy to achieve because of plug formation or channeling in the bed. It should be noted that Eq. 13, which we have used for the transition between group A and C particles, is based on the assumption that group C particles cannot be fluidized individually and group A particles can. Thus the essential characteristic of group C particles is that they are in the agglomerating fluidization regime.

The major difference between group A and B particles is whether bubbles appear at the minimum fluidization velocity

or after the minimum fluidization velocity is reached. For both groups relatively stable fluidization is obtained. Thus both group A and B particles give rise to stable fluidization.

Geldart (1973) obtained an equation for the transition of group B to group D by calculating the density/particle-size combination of powders in which bubbles less than a given size would rise more slowly than the interstitial gas velocity. He chose a very large bubble size (25 cm) in his calculation. Molerus (1982) developed his semiempirical equation for the transition between group B and D from spouted-bed data. Beds exhibiting very large bubbles or spouted bed are both unstable fluidized beds. Thus group D particles exhibit unstable fluidization.

Based on the definitions given previously, we can rearrange Eqs. 13 and 18 to give

$$(\rho_p - \rho_f)\frac{g}{9.8} = \frac{Al}{24\delta^2}\frac{6}{\pi d_p^3}\frac{1}{(\epsilon^{-4.8} - \epsilon)}\frac{1}{9.8} \qquad (19)$$

$$(\rho_p - \rho_f)\frac{g}{9.8} = \frac{15.3}{d_p}\frac{1}{9.8}, \qquad (20)$$

where $g/9.8$ represents the dimensionless strength of the centrifugal field ("g"). As already pointed out earlier, Eq. 20 was derived based on the assumption that $Re \gg 1$.

If we plot the lefthand side of Eqs. 19 and 20 as the ordinate and d_p as the abscissa, we obtain Figure 17. This figure shows the effect of different "g" conditions, such as that on the earth, on the moon, in a centrifugal field, and in deep space on the powder classification chart. We have taken the gravity on the moon to be 0.17 times that of the earth. Here we are assuming that particles in group A and B (region AB) will result in stable fluidization. Thus, if we choose particles of density 1 g/cm^3, the figure indicates that particles between 60 and 10,000 μm would achieve stable fluidization on the moon, whereas particles between 30 and 1,500 μm would achieve stable fluidization on the earth. For rotating fluidized beds, the figure shows that it will be difficult to achieve stable fluidization at over 100 "g" except in a very narrow particle-size range.

The figure also shows our experimental data for 7-μm alumina, washed alumina, glass beads, and Q-705 alumina. The observed fluidization behavior for these particles is indicated by the symbol type, as shown in the figure. The 7-μm alumina data appear to be consistent with the transition curves, even though $Re \approx 1$. The lower two data points exhibit group C behavior, the middle two represent stable fluidization (AB), and the upper two show group-D-like behavior.

In all experiments conducted with larger particles (60 ~ 90 μm), stable fluidization (AB) was achieved even though many of the experimental data points fall above the AB/D transition curve. Again for these experiments typical Reynolds numbers are on the order of unity, for which the AB/D transition curve drawn in the figure may not apply.

Therefore further investigation of the AB/D transition in rotating fluidized beds is needed.

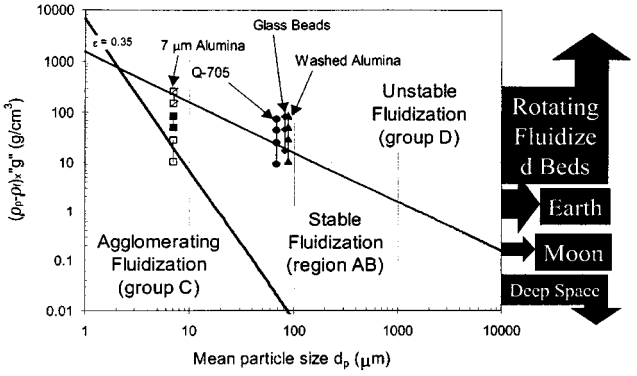

Figure 17. Powder classification for fluidization by air at different " *g*."

open = group C; solid = region AB; slashed = group D-like.

Acknowledgments

This research was supported by the National Science Foundation under Grant No. CTS-9612483. The authors express their appreciation to W. Weissman (ExxonMobil) and Dr. Rajesh N. Dave (Mechanical Engineering Department, NJIT) for their valuable suggestions and discussions.

Notation

a = acceleration, m/s^2
A = Hamaker constant, J (for most solids, $A \approx 10^{-19}$ J)
C_D = drag coefficient
d_i = diameter of particle i ($i = 1, 2$), m
d_p = particle diameter, m
D_t = bed diameter, m
Eu_{mf} = Euler number at minimum fluidization, defined by Eq. 15
F_c = cohesive force, N
F_d = drag force on a single isolated particle, N
F_{dt} = drag force on a single particle falling at its terminal velocity, N
$F_{d\epsilon}$ = drag force on a single particle in a fluidized bed, N
g = gravitational acceleration, m/s^2
"g" = dimensionless acceleration, "g" = a/(9.8 m/s^2)
l = diameter of asperities, μm
n = exponent in Richardson-Zaki equation
Re = particle Reynolds number $Re = (\rho_f d_p u/\epsilon\mu)$
Re_t = Reynolds number for unhindered settling particle $Re_t = (\rho_f/d_p u_t/\mu)$
u, U_g = superficial gas velocity, m/s
u_m = maximum gas velocity before particles blow out, m/s
u_t = particle terminal velocity, m/s
U_{mf} = minimum fluidization velocity, m/s
U_{mb} = minimum bubbling velocity, m/s
U_{mfc} = critical minimum fluidization velocity, m/s
U_{mfi} = inner surface minimum fluidization velocity, m/s
W_b = buoyancy force, N
W_e = effective weight of particle, N
W_g = weight of particle, N

Greek letters

ΔP = pressure drop across the bed, Pa
ϵ = voidage
ϵ_b = voidage at the transition from particulate to aggregative fluidization
ϵ_{mb} = voidage at minimum bubbling condition
ϵ_{mf} = voidage at minimum fluidization condition
μ = fluid viscosity, Pa·s
ρ_a = density of "suspension," kg/m^3
ρ_f = gas density, kg/m^3
ρ_p = particle density, kg/m^3
δ = distance between two particles, nm
ω = rotating speed, rad/s

Literature Cited

Chaouki, J., C. Chavarie, and D. Klvana, ''Effect of Interparticle Forces on the Hydrodynamic Behavior of Fluidized Aerogels,'' *Powder Technol.*, **43**, 117 (1985).

Chen, Y., ''Fundamentals of a Centrifugal Fluidized Bed,'' *AIChE J.*, **33**, 722 (1987).

Chirone, R., L. Massimilla, and S. Russo, ''Bubbling Fluidization of a Cohesive Powder in an Acoustic Field,'' *Fluidization VII*, O. E. Potter and D. J. Nicklin, eds., Engineering Foundation, New York, p. 545 (1992).

Fan, L. T., C. C. Chang, Y. S. Yu, T. Takahashi, and Z. Tanaka, ''Incipient Fluidization Condition for a Centrifugal Fluidized Bed,'' *AIChE J.*, **31**, 999 (1985).

Foscolo, P. U., and L. G. Gibilaro, ''A Fully Predictive Criterion for the Transition Between Particulate and Aggregate Fluidization,'' *Chem. Eng. Sci.*, **39**, 1667 (1984).

Geldart, D., ''Types of Gas Fluidization,'' *Powder Technol.*, **7**, 285 (1973).

Geldart, D., and A. R. Abrahamsen, ''The Effect of Fines on the Behavior of Gas Fluidized Beds of Small Particles,'' *Fluidization*, J. R. Grace and J. M. Matsen, eds., Plenum Press, New York, p. 453 (1980).

Iwadate, Y., and M. Horio, ''Prediction of Agglomerate Sizes in Bubbling Fluidized Beds of Group C Powders,'' *Powder Technol.*, **100**, 223 (1998).

Jackson, R., ''The Mechanics of Fluidized Beds,'' *Trans. Inst. Chem. Eng.*, **41**, 13 (1963).

Kao, J., R. Pfeffer, and G. I. Tardos, ''On Partial Fluidization in Rotating Fluidized Beds,'' *AIChE J.*, **33**, 858 (1987).

Khan, A. R., and J. F. Richardson, ''Pressure Gradient and Friction Factor for Sedimentation and Fluidization of Uniform Spheres in Liquids,'' *Chem. Eng. Sci.*, **45**(1) 255 (1990).

Kroger, D. G., G. Abdelnour, E. K. Levy, and J. C. Chen, ''Particle Distribution and Mixing in a Centrifugal Fluidized Bed,'' *Fluidization*, J. R. Grace and J. M. Matsen, eds., Plenum Press, New York, p. 349 (1980).

Krupp, H., ''Particle Adhesion, Theory and Experiment,'' *Adv. Colloid Interface Sci.*, **1**, 111 (1967).

Levy, E. N., N. Martin, and J. Chen, ''Minimum Fluidization and Startup of a Centrifugal Fluidized Bed,'' *Fluidization*, D. L. Kearins, ed., Cambridge Univ. Press, Cambridge, p. 71 (1978).

Levy, E. K., W. J. Shakespeare, A. Tabatabaie-Raissi, and J. C. Chen, ''Particle Elutriation from Centrifugal Fluidized Beds,'' *Recent Advances in Fluidization, AIChE Symp. Ser.*, **77** (205), 86 (1981).

Massimilla, L., and G. Donsi, ''Cohesive Forces Between Particles of Fluid-Bed Catalysts,'' *Powder Technol.*, **15**, 253 (1976).

Mathur, K. B., ''Spouted Beds,'' *Fluidization*, Chap. 17, J. F. Davidson and D. H. Harrison, eds., Academic Press, London (1971).

Molerus, O., ''Interpretation of Geldart's Type A, B, C and D Powders by Taking into Account Interparticle Cohesion Forces,'' *Powder Technol.*, **33**, 81 (1982).

Mori, S., N. Iwasaki, E. Mizutani, and T. Okada, ''Vibro-Fluidization of Two-Component Mixtures of Group C Particles,'' *Fluidization VII*, O. E. Potter and D. J. Nicklin, eds., Engineering Foundation, New York, p. 571 (1992).

Mutsers, S. M. P., and K. Rietema, ''The Effect of Interparticle Forces on the Expansion of a Homogeneous Gas-Fluidized Bed,'' *Powder Technol.*, **18**, 239 (1977a).

Mutsers, S. M. P., and K. Rietema, ''Gas-Solids Fluidization in a Centrifugal Field. The Effect of Gravity upon Bed Expansion,'' *Powder Technol.*, **18**, 249 (1977b).

Oltrogge, R. D., PhD Thesis, Univ. of Michigan, Ann Arbor (1972).

Qian, G. H., I. Bágyi, R. Pfeffer, H. Shaw, and J. G. Stevens, ''A Parametric Study of a Horizontal Rotating Fluidized Bed Using Slotted and Sintered Metal Cylindrical Gas Distributors,'' *Powder Technol.*, **100**, 190 (1998).

Qian, G. H., I. Bágyi, R. Pfeffer, H. Shaw, and J. G. Stevens, ''Particle Mixing in Rotating Fluidized Beds: Inferences about the Fluidized State,'' *AIChE J.*, **45**, 1401 (1999).

Richardson, J. F., and W. N. Zaki, ''Sedimentation and Fluidization: Part I,'' *Trans. Inst. Chem. Eng.*, **32**, 35 (1954).

Rietema, K., ''The Effect of Interparticle Forces on the Expansion of a Homogeneous Gas-Fluidized Bed,'' *Chem. Eng. Sci.*, **28**, 1493 (1973).

Rietema, K., ''Powders, What Are They?'' *Powder Technol.*, **37**, 5 (1984).

Rietema, K., E. J. E. Cottaar, and H. W. Piepers, ''The Effect of Interparticle Forces on the Stability of Gas-Fluidized Beds—II. Theoretical Derivation of Bed Elasticity on the Basis of van der Waals Forces Between Powder Particles,'' *Chem. Eng. Sci.*, **48**(9), 1687 (1993).

Schlichting, H., *Boundary Layer Theory*, 7th ed., McGraw-Hill, New York (1979).

Tung, Y., and M. Kwauk, ''Assessing Fluidizing Characteristics of Powders,'' *Proc. of the Int. Conf. on Fluidization*, J. R. Grace, ed., Banff, Canada, p. 169 (1989).

Verloop, J., and P. M. Heertjes, ''Shock Waves as a Criterion for the Transition from Homogeneous to Heterogeneous Fluidization,'' *Chem. Eng. Sci.*, **25**, 825 (1970).

Wallis, G. B., *One-Dimensional Two-Phase Flow*, McGraw-Hill, New York (1969).

Wang, Z., M. Kwauk, and H. Li, ''Fluidization of Fine Particles,'' *Chem. Eng. Sci.*, **53**, 377 (1998).

Wilhelm, R. H., and M. Kwauk, ''Fluidization of Solid Particles,'' *Chem. Eng. Prog.*, **44**, 201 (1948).

Zhou, T., and H. Li, ''Estimation of Agglomerate Size for Cohesive Particles During Fluidization,'' *Powder Technol.*, **101**, 57 (1999).

Manuscript received Feb. 28, 2000, and revision received Oct. 17, 2000.